J. Phys. D: Appl. Phys. **30** (1997) 2663–2676. Printed in the UK PII: S0022-3727(97)81741-X

Self-consistent kinetic model of a surface-wave-sustained discharge in nitrogen

E Tatarova†§, F M Dias†, C M Ferreira†, V Guerra†, J Loureiro†, E Stoykova‡, I Ghanashev‡ and I Zhelyazkov‡

† Centro de Electrodinâmica, Instituto Superior Técnico, Universidade Técnica de Lisboa, P-1096 Lisboa Codex, Portugal
‡ Faculty of Physics, Sofia University, BG-1164 Sofia, Bulgaria

Received 10 February 1997

Abstract. A self-consistent kinetic model based on a set of coupled equations consisting of the local electron Boltzmann equation and the rate balance equations for the most important excited species (vibrationally and electronically excited molecular states) and charged particles in a nitrogen discharge has been developed. The system under analysis is a plasma column produced by a travelling, azimuthally symmetric surface wave. Electron collisions of first and second kind with nitrogen molecules and electron–electron collisions are accounted for in the Boltzmann equation. Therefore, this equation is coupled to the set of equations for electronic and vibrational populations through both inelastic and superelastic collisions. The field strength necessary for the discharge steady-state operation is obtained from the balance between the total rate of ionization (including associative, direct and step-wise ionization) and the total rate of electronic losses (due to diffusion to the wall and bulk recombination). The model determines, as a function of the discharge operating parameters (pressure, tube radius, wave frequency, degree of ionization), the electron energy distribution, the populations of the vibrational levels of the electronic ground state and the most important electronic states $N_2(A\,^3\Sigma_u^+, a'\,^1\Sigma_u^-, B\,^3\Pi_g, a\,^1\Pi_g, C\,^3\Pi_u)$ as well as the concentrations of N_2^+ and N_4^+ ions, consistently with the discharge maintaining electric field. Theoretical results for the electron energy distribution function and some of its moments are compared with experimental ones obtained in a low-pressure surface-wave-sustained discharge at a wave frequency of 500 MHz.

1. Introduction

Among the variety of high-frequency-produced discharges, a plasma column sustained by a travelling, azimuthally symmetric electromagnetic surface wave is certainly one of the most well behaved HF plasmas [1]. The surface wave field heats the electrons which ionize the gas ensuring in this way the wave propagation; the plasma column so generated acts as a self-supporting waveguide. This means that the surface wave (SW) plasmas do not require an accompanying waveguide structure placed all the way along the plasma column because the wave generates its own propagation structure. Aside from the technological aspects which make SW plasmas attractive for applications [1], the SW plasmas exhibit some properties which considerably simplify theoretical calculations. For instance, in the limit of the 'long-wavelength approximation', valid in a given range of discharge conditions, the SW electric field maintaining the discharge may be considered as radially homogeneous [2, 3].

Regarding present knowledge on SW sustained discharges, it is noteworthy that SW plasma physics has reached a modelling stage (in the case of inert gases) far above that for any other HF plasmas. But, despite the good deal of theoretical and experimental work [2–17] which has been done in recent years, the more complicated cases of molecular gases, important for applications, have been much less investigated. The principal reason for this is that the elementary processes in molecular gases are complex and depend on many, strongly coupled parameters.

Nitrogen is widely used in gas discharge physics investigations and applications, one of the reasons being that it has a number of states that store energy and make it available for specific processes [18]. These states, which include vibrationally and electronically excited states of nitrogen molecules, atoms, etc, are essential for applications. Theoretical investigations of nitrogen plasmas have clarified many interesting properties. The electron energy distribution function is generally non-

§ On leave from Faculty of Physics, Sofia University, BG-1164 Sofia, Bulgaria. E-mail address: elt@phys.uni-sofia.bg

Maxwellian, its form reflects important features of the electron–molecule energy exchange processes. Superelastic collisions between electrons and vibrationally excited molecules in the electronic ground state $N_2(X\,^1\Sigma_g^+)$ play an important role in enhancing the electron energy spectrum at high energies [19]. Knowledge of the distribution of vibrationally excited molecules is therefore essential to estimate the influence of these collisions. Loureiro and Ferreira [20–22] have reported self-consistent calculations based on the Boltzmann equation with inelastic and superelastic collisions coupled to vibrational rate balance equations including electron–vibration (e–V), vibration–vibration (V–V) and vibration–translation (V–T). Capitelli, Winkler and co-workers [23–26] have investigated the problem of the time evolution of the coupled electron energy distribution function (EEDF) and vibrational distribution function (VDF) for the bulk plasma in RF discharges. The solution to the coupled electron and vibrational kinetic equations in N_2 discharges has provided detailed qualitative insight into the discharge energy balance and the relative importance of various electron and heavy-particle collisional processes. However, the basic point of interest in modelling nitrogen discharges (keeping in mind technological purposes) is to correctly predict the population densities of all heavy particles, consistently with the electron energy distribution and the electric field sustaining the discharge, as a function of the discharge operating conditions (pressure, wave frequency, vessel geometry, degree of ionization or absorbed power). The main plasma processes depend on the properties of the discharge which, in turn, are determined by the externally controllable system design and operating parameters. It should be emphasized that to optimize plasma processes the knowledge of general trends is more important than a 'specific solution' to a particular case.

For the above reasons, a self-consistent kinetic model based on the set of coupled equations consisting of the local electron Boltzmann equation and the rate balance equations for the most important excited species (vibrationally and electronically excited molecular states) and charged particles in the discharge has been developed in the present work. The system under analysis is a plasma column produced by a surface wave (in the azimuthally symmetric mode) in the limit of the 'long-wavelength approximation'. Electron collisions of first and second kind with nitrogen molecules and electron–electron collisions are accounted for in the Boltzmann equation which is therefore coupled to the set of equations for electronic and vibrational populations through both inelastic and superelastic collisions. The field strength necessary for a steady-state operation of the discharge is obtained from the balance between the total rate of ionization, including associative (from $N_2(A\,^3\Sigma_u^+)$ and $N_2(a'\,^1\Sigma_u^-)$ metastable states), direct and step-wise ionization (from $N_2(A\,^3\Sigma_u^+)$, $N_2(a'\,^1\Sigma_u^-)$, and $N_2(B\,^3\Pi_g)$ states), and the total rate of electronic losses (due to diffusion to the wall and bulk recombination). A boundary condition for the ion speed is applied in order to account for the sheath formation at the wall.

The model determines, as a function of discharge operating parameters, the EEDF, the radially averaged populations of the vibrational levels of the electronic ground state and the most important electronic states $N_2(A\,^3\Sigma_u^+, a'\,^1\Sigma_u^-, B\,^3\Pi_g, a\,^1\Pi_g, C\,^3\Pi_u)$ as well as the concentrations of N_2^+ and N_4^+ ions, consistently with the discharge maintaining electric field. Theoretical results for the EEDF and some of its moments are compared with experimental ones obtained in a surface-wave-produced nitrogen discharge at $\omega/2\pi = 500$ MHz.

The paper is organized as follows. Details on the model and input data are presented in section 2. Results describing electron and heavy-particle kinetics are given in section 3. The comparison with experimental data is made in section 4. Section 5 is devoted to the main conclusions.

2. Theoretical formulation

The situation to be considered here is that of a plasma column of radius R sustained by a travelling surface wave.

2.1. 'Long-wavelength approximation'

An azimuthally symmetric surface wave possesses both radial, E_r, and axial, E_z, electric field components with radial variations in their amplitudes. Since in the bulk plasma $|E_z(r)| > |E_r(r)|$, the E_z field component is the main contributor to the total surface wave electric field. Concerning the electric field radial profile we assume the validity of the *long-wavelength approximation*, also called *thin-cylinder approximation* [27]. As pointed out in [2, 3, 28], in this approximation the electric field is nearly constant over the whole radius

$$|E(r)| \cong |E_z(r)| \cong \text{constant}$$

which considerably simplifies the kinetic modelling of surface-wave-produced plasmas in this case. The criterion for validity of this approximation may be formulated as [3]

$$|k_\perp R| < 1$$

where $k_\perp$ is the transverse wavenumber, a complex/imaginary quantity which determines the 'reciprocal radial decay length' of the electric field. For the collisionless case (when $\nu_{en} \ll \omega$ with ν_{en} being the electron–neutral elastic collision frequency)

$$|k_\perp| = [\beta^2 - (\omega/c)^2 \varepsilon_{pl}]^{1/2}$$

where $\varepsilon_{pl} \cong 1 - (\omega_{pe}/\omega)^2$ is the plasma permittivity, ω_{pe} and β are the electron plasma frequency and the axial wavenumber respectively. Estimations show that for electron number densities $n_e \in 10^{16}$–10^{17} m^{-3}, wavenumbers $\beta \in 60$–80 m^{-1} ($\omega/2\pi = 200$ MHz, $R = 2$ cm) the 'long-wavelength approximation' is valid. However, for densities $n_e > 10^{17}$ m^{-3}, due to large values of ε_{pl} this approximation is violated. As emphasized in [3], the range of validity of the 'thin-cylinder approximation' towards higher densities is considerably extended if collisional effects are accounted for. In fact, it has been shown that collisions yield a significant flattering in the E_z radial profile even for low values

of the ratio ν_{en}/ω. For this reason, in order to study basic trends, the numerical calculations in the present investigation are extended to electron densities of the order of 10^{18} m^{-3}. Thus, we assume that the surface wave electric field maintaining the discharge may be considered radially homogeneous and directed along the plasma axis, $\boldsymbol{E} = \hat{z}E\exp(\mathrm{i}\omega t)$.

2.2. Boltzmann equation

Calculations were made by numerically solving the steady-state electron Boltzmann equation using the classical two-term expansion in spherical harmonics. We assume the following:

(i) the field amplitude and the diffusion gradients are sufficiently small that the anisotropy of the electron velocity distribution remains low and the latter distribution can be well represented by a two-term expansion in spherical harmonics;

(ii) the wave frequency ω is sufficiently high so that the electrons do not lose appreciable energy in collisions during a cycle of the field oscillation and the EEDF can be assumed stationary;

(iii) the space charge field is small and can be neglected, i.e. the electron energy distribution is essentially determined by the external HF field and the energy losses associated with inelastic and elastic collisions, thus the local approximation is valid;

(iv) the effects of secondary electron production can be neglected.

Under the above assumptions, the fundamental equation obtained for the EEDF is [2, 21, 29–31]:

$$\begin{aligned}
&-\frac{\mathrm{d}}{\mathrm{d}u}\left\{\left[\frac{1}{3}\left(\frac{E_{\mathrm{eff}}}{N}\right)^2\frac{u}{Q_{en}}+2F_{ee}\frac{n_e}{N}g(u)\right]\frac{\mathrm{d}f_0}{\mathrm{d}u}\right.\\
&\qquad\left.+\left[kQ_{en}u^2+3F_{ee}\frac{n_e}{N}h(u)\right]f_0(u)\right\}\\
&\quad=\sum_{i,j}\delta_i\{(u+u_{ij})q_{ij}(u+u_{ij})\,f_0(u+u_{ij})\\
&\qquad-uq_{ij}(u)\,f_0(u)\}+\sum_{j,i}\delta_j\{(u-u_{ij})q_{ji}(u-u_{ij})\\
&\qquad\times f_0(u-u_{ij})-uq_{ji}(u)\,f_0(u)\}
\end{aligned}\tag{1}$$

where $f_0(u)$ is normalized as

$$\int_0^\infty f_0(u)\sqrt{u}\,\mathrm{d}u=1.$$

Here, u is the electron energy in eV, E_{eff} is the effective electric field

$$E_{\mathrm{eff}}=\frac{E}{\sqrt{2}}\frac{\nu_{en}(u)}{\left(\nu_{en}^2(u)+\omega^2\right)^{1/2}}$$

and

$$F_{ee}=\frac{e^2}{24\pi\varepsilon_0^2}\ln\Lambda\qquad\Lambda=12\pi\left(\tfrac{2}{3}\langle u\rangle\varepsilon_0 e\right)^{3/2}e^{-3}n_e^{-1/2}$$

$$g(u)=\int_0^u x^{3/2}f_0(x)\,\mathrm{d}x+u^{3/2}\int_u^\infty f_0(x)\,\mathrm{d}x$$

$$h(u)=\int_0^u x^{1/2}f_0(x)\,\mathrm{d}x.$$

Herein, N is the total neutral number density, $\langle u\rangle$ is the mean electron energy, e is the elementary electric charge, and $k=2m/M$, where m and M denote the electron and molecular mass respectively. The total momentum transfer cross-section $Q_{en}(u)$ includes the contributions of electron–molecule and electron–ion collisions [29].

The first term on the right-hand side of (1) accounts for collisions of the first kind in which an electron gives internal energy to a nitrogen molecule; q_{ij} is the cross-section for excitation from the ith to the jth state, u_{ij} denoting the corresponding energy threshold; and $\delta_i = N_i/N$ is the relative concentration of N_2 molecules in the ith level. The second term accounts for collisions of the second kind (superelastic collisions) in which an excited molecule supplies energy to the colliding electron; q_{ji} is the electronic cross-section for de-excitation from the jth to the ith state.

The excitation of electronic states was treated as a single energy loss process assuming that all molecules are in the ground vibrational level $\mathrm{N}_2(\mathrm{X}\,^1\Sigma_g^+, v=0)$, i.e. no discrimination has been made in this case between individual vibrational levels of the ground and the final electronic states. Further on, (1) treats the ionization process similarly to an excitation with a single energy loss, equal to the ionization energy, and neglects the production of new electrons by direct ionization. In the calculations, superelastic collisions of electrons with electronically excited states were neglected since, in general, $\delta_i \ll 1$ for these states. Thus, only excitation and ionization from the ground state are considered. In this case, on the right-hand side of equation (1) the contribution of excitation to electronic states reduces to

$$\sum_{s=1}^{9}\{(u+u_s)q_s(u+u_s)\,f_0(u+u_s)-uq_s(u)\,f_0(u)\}$$

with the subscript s referring to various states. Consequently, the δ_i's appearing in the remaining terms refer only to the fractional populations in the vibrational levels of the electronic ground state, $\delta_v = N_v/N$, N_v denoting the number density of vibrationally excited molecules in the vth level. Vibrationally excited molecules in an electric discharge may constitute an appreciable fraction of the total molecular population. Thus the EEDF is strongly affected by their presence, as is well-known.

On inspection of equation (1) is seen that the EEDF depends on the set of parameters E/N, ω/N, n_e/N, N_v/N. The degree of ionization n_e/N can be obtained from measurements and be considered as an independent parameter, since it can be externally controlled by changing the power supplied to the discharge. In general, $f_0(u)$ is a function of the vibrational distribution function $\delta_v = N_v/N$ and the electric field maintaining the discharge, so a self-consistent determination is of particular importance. The inelastic and superelastic processes included in the electron Boltzmann equation as well as the sources of data are given in table 1. The cross-section for direct electron impact ionization, with appropriate shifts in the energy scale, was used for step-wise ionization processes.

Table 1. Inelastic and superelastic electron collisions.

Process	Rate constant	Reference
$e + N_2(X\,^1\Sigma_g^+, v = i) \rightarrow N_2(X\,^1\Sigma_g^+, v = j) + e$ with $i, j = 0$–8, $i < j$		[32]
$e + N_2(X\,^1\Sigma_g^+, v = j) \rightarrow N_2(X\,^1\Sigma_g^+, v = i) + e$ with $i, j = 0$–8, $i < j$		[32]
$e + N_2(X\,^1\Sigma_g^+, v = 0) \rightarrow N_2(Y) + e$ for $Y = (A\,^3\Sigma_u^+, a'\,^1\Sigma_u^-, B\,^3\Pi_g, a\,^1\Pi_g, C\,^3\Pi_u, B'\,^3\Sigma_u^-, W\,^3\Delta_u, E\,^3\Sigma_g^+)$		[32]
$e + N_2(X\,^1\Sigma_g^+, v = 0) \rightarrow N_2^+ + e + e$	Z_1	[32]
$e + N_2(A\,^3\Sigma_u^+) \rightarrow N_2^+ + e + e$	Z_2	[32]
$e + N_2(B\,^3\Pi_g) \rightarrow N_2^+ + e + e$	Z_3	[32]
$e + N_2(a'\,^1\Sigma_u^-) \rightarrow N_2^+ + e + e$	Z_4	[32]

2.3. Heavy-particle kinetics

2.3.1. Vibrational distribution function δ_v. Since the EEDF is a function of the vibrational distribution function, the latter must be obtained consistently with $f_0(u)$ by coupling (1) to the set of rate balance equations for the vibrational population of the electronic ground state. The vibrational master equations can be written in a symbolic form as [20–26, 33, 34]

$$\left(\frac{\mathrm{d}N_v}{\mathrm{d}t}\right)_{e-V} + \left(\frac{\mathrm{d}N_v}{\mathrm{d}t}\right)_{V-V} + \left(\frac{\mathrm{d}N_v}{\mathrm{d}t}\right)_{V-T} + \left(\frac{\mathrm{d}N_v}{\mathrm{d}t}\right)_{V-T}^{N_2-N} + \left(\frac{\mathrm{d}N_v}{\mathrm{d}t}\right)_{W} + \left(\frac{\mathrm{d}N_v}{\mathrm{d}t}\right)_{e-D} + \left(\frac{\mathrm{d}N_v}{\mathrm{d}t}\right)_{V-D} + \left(\frac{\mathrm{d}N_v}{\mathrm{d}t}\right)_{R} = 0. \quad (2)$$

The various processes accounted for in equation (2) are listed in table 2. We note that only single quantum transitions, which are the most likely ones, have been considered in the V–V and V–T collisional exchange processes. The sole exception concerns V–T exchanges in N_2–N collisions in which the effects of multiquantum transitions are known to be important [33, 34]. The V–D reactions take into account dissociation by V–V and V–T processes which is modelled as a transition from the last bound level $v = 45$ to a pseudo-level in the continuum [23–25].

The equations and mechanisms accounted for are in full discussed in [33–35] and the reader should refer to these papers for further details.

2.3.2. Electronically excited molecules. It has been found to be important to include in the model associative ionization involving $N_2(A\,^3\Sigma_u^+)$ and $N_2(a'\,^1\Sigma_u^-)$ states and step-wise ionization from $N_2(A\,^3\Sigma_u^+)$, $N_2(a'\,^1\Sigma_u^-)$, and $N_2(B\,^3\Pi_g)$ states. Thus, in addition to all electron impact and vibrational kinetic processes the model includes reactions determining the population densities of five excited electronic states $N_2(A\,^3\Sigma_u^+, a'\,^1\Sigma_u^-, B\,^3\Pi_g, C\,^3\Pi_u, a\,^1\Pi_g)$. Assuming that the radial profile of excited particles is a zero-order Bessel function, the rate equations are deduced by taking into account the collisional and radiative processes given in tables 1 and 3.

The metastable particles $N_2(A\,^3\Sigma_u^+)$ and $N_2(a'\,^1\Sigma_u^-)$ are mainly produced by direct excitation (table 1) and by transition from the $N_2(B\,^3\Pi_g)$, $N_2(a\,^1\Pi_g)$ and $N_2(C\,^3\Pi_u)$ states. They are lost by diffusion to the wall (the diffusion coefficient D_m is given by $49 \times 10^{-4}/p$ m^2 s^{-1}, where the pressure p is in Torr [42]) and by transitions to other levels. Another important loss mechanism for $N_2(A\,^3\Sigma_u^+)$ comes from collisions with nitrogen atoms. The relative density of nitrogen atoms is not determined from our model and has been assumed to be 1%, which is a typical value under present conditions.

2.3.3. Density of positive ions. In the present work we consider three species of charged particles: electrons and two kinds of positive ion, N_2^+ and N_4^+, respectively. The charged particle concentrations are assumed to obey the quasineutrality condition

$$n_e = \sum_{j=1}^{2} N_j.$$

Hereafter, the subscripts $j = 1, 2$ will be used to identify data related to N_2^+ ($j = 1$) and N_4^+ ($j = 2$) correspondingly.

The N_2^+ ions are created by electron impact ionization of neutral molecules, step-wise ionization (table 1) and associative ionization (table 4), while N_4^+ ions are born mainly due to associative ionization processes involving $N_2(A\,^3\Sigma_u^+)$ and $N_2(a'\,^1\Sigma_u^-)$ metastable states. Due to the lack of data, we assume the same branching ratio for the production of N_2^+ and N_4^+ by associative ionization. Additional channels contributing to the appearance or the removal of positive ions are also listed in table 4. The main processes of removal of charged particles are the ambipolar diffusion to the wall and bulk dissociative recombination (table 5). Electron rate coefficients for dissociative recombination of N_2^+ and N_4^+ have been calculated using semi-empirical formulae reported in [37] as a function of the electron temperature T_e.

Assuming quasineutrality, ambipolar flow conditions $n_e V_e = \sum N_j V_j$, and proportionality $\nabla n_e / n_e \cong \nabla N_j / N_j$, we can express the transport of charged particles to the wall in terms of ambipolar diffusion coefficients, correspondingly given by [47]

$$D_{ae} = \frac{D_e \sum_j N_j \mu_j + \mu_e \sum_j N_j D_j}{\sum_j N_j \mu_j + n_e \mu_e}$$

Table 2. Kinetics of $N_2(X\,^1\Sigma_g^+)$ molecules.

Notation	Process
e–V	$e + N_2(X\,^1\Sigma_g^+, v) \Leftrightarrow e + N_2(X\,^1\Sigma_g^+, w)$
V–V	$N_2(X\,^1\Sigma_g^+, v) + N_2(X\,^1\Sigma_g^+, w) \Leftrightarrow N_2(X\,^1\Sigma_g^+, v-1) + N_2(X\,^1\Sigma_g^+, w+1)$
V–T	$N_2(X\,^1\Sigma_g^+, v) + N_2 \Leftrightarrow N_2(X\,^1\Sigma_g^+, v-1) + N_2$
V–T (N_2–N)	$N_2(X\,^1\Sigma_g^+, v) + N \Leftrightarrow N_2(X\,^1\Sigma_g^+, w < v) + N$
	$N_2(X\,^1\Sigma_g^+, v) + N \Leftrightarrow N + N_2(X\,^1\Sigma_g^+, w < v)$
W	$N_2(X\,^1\Sigma_g^+, v) + \text{wall} \rightarrow N_2(X\,^1\Sigma_g^+, v-1)$
e–D	$e + N_2(X\,^1\Sigma_g^+, v) \rightarrow e + N + N$
V–D	$N_2(X\,^1\Sigma_g^+, v) + N_2(X\,^1\Sigma_g^+, v=45) \rightarrow N_2(X\,^1\Sigma_g^+, v-1) + N + N$
	$N_2 + N_2(X\,^1\Sigma_g^+, v=45) \rightarrow N_2 + N + N$
R	$N + N \rightarrow N_2(X\,^1\Sigma_g^+, v=0)$

Table 3. Collisional–radiative processes involving electronically excited molecules.

Process	k ($m^3\ s^{-1}$)	References
$N_2(a'\,^1\Sigma_u^-) + N_2(X) \rightarrow N_2(B\,^3\Pi_g) + N_2(X)$	1.9×10^{-19}	[36, 37]
$N_2(C\,^3\Pi_u) + N_2(X) \rightarrow N_2(a'\,^1\Sigma_u^-) + N_2(X)$	1.0×10^{-17}	[35, 38, 39]
$N_2(a\,^1\Pi_g) + N_2(X) \rightarrow N_2(a'\,^1\Sigma_u^-) + N_2(X)$	2.0×10^{-17}	[40]
$N_2(a\,^1\Pi_g) \rightarrow N_2(a'\,^1\Sigma_u^-) + hf$	$1.91 \times 10^{2}\ s^{-1}$	[41]
$N_2(C\,^3\Pi_u) \rightarrow N_2(B\,^3\Pi_g) + hf$	$13.9 \times 10^{6}\ s^{-1}$	[42]
$N_2(B\,^3\Pi_g) \rightarrow N_2(A\,^3\Sigma_u^+) + hf$	$6.25 \times 10^{4}\ s^{-1}$	[42]
$N_2(B\,^3\Pi_g) + N_2 \rightarrow N_2(X) + N_2$	3.0×10^{-17}	[43]
$N_2(A\,^3\Sigma_u^+) + N_2(X) \rightarrow 2N_2$	3.0×10^{-22}	[44]
$N_2(A\,^3\Sigma_u^+) + N \rightarrow N_2(X) + N$	5.0×10^{-17}	[45]
$N_2(a\,^1\Pi_g) \rightarrow N_2(X) + hf$	$1.8 \times 10^{4}\ s^{-1}$	[40]

$$D_{aj} = \frac{(D_j \sum_j N_j\mu_j - \mu_j \sum_j N_j D_j) + n_e(\mu_j D_e + \mu_e D_j)}{\sum_j N_j\mu_j + n_e\mu_e}.$$

Here, D_j is the ion free diffusion coefficient, μ_j and μ_e are the ion and electron mobility respectively. The mobilities μ_j are obtained from data for the reduced mobility of nitrogen ions given in [48].

2.4. Method of solution

For a self-consistent determination of the HF field, a balance between the rates of charged particle production and loss has to be obeyed. Thus, following [7, 35, 49] the field strength necessary for a steady-state operation of the discharge is obtained from the balance between the total rate of ionization, including direct, associative (involving $N_2t(A\,^3\Sigma_u^+)$ and $N_2(a'\,^1\Sigma_u^-)$) and step-wise ionization (from $N_2(A\,^3\Sigma_u^+)$, $N_2(a'\,^1\Sigma_u^-)$, and $N_2(B\,^3\Pi_g)$) processes and the total rate of electronic losses due to diffusion to the wall and bulk recombination. Taking into account the ionization and recombination processes described in tables 1, 3, 4, 5 alongside corresponding rate coefficients, the electrons satisfy the following continuity equation:

$$\begin{aligned} &n_e N Z_1 + n_e N(\mathrm{A}) Z_2 + n_e N(\mathrm{B}) Z_3 + n_e N(\mathrm{a}') Z_4 \\ &\quad + N(\mathrm{a}') N(\mathrm{A}) K_{as1} + N(\mathrm{a}')^2 K_{as2} \\ &= n_e \frac{D_{ae}}{\Lambda_{\mathrm{eff}}^2} + \alpha_{r1} n_e N_1 + \alpha_{r2} n_e N_2 \end{aligned} \tag{3}$$

where the symbols A, a′, and B denote $N_2(A\,^3\Sigma_u^+)$, $N_2(a'\,^1\Sigma_u^-)$, and $N_2(B\,^3\Pi_g)$ states respectively, and Z_l ($l = 1, 2, 3, 4$) are the corresponding rate coefficients (see table 1). Λ_{eff} is an effective diffusion length which was determined assuming that ions of each type reach the corresponding ion sound speed at the plasma–sheath boundary. Although such an assumption is not fully correct in the presence of several types of ion [50], it has little effect here on the results since N_2^+ is largely dominant as compared to N_4^+ in our case (see below).

The former set of equations was solved in a self-consistent manner. Equation (1) is an ordinary nonlinear differential equation. It is linearized by an iterative procedure and converted into a set of coupled algebraic equations by subdividing the electron energy axis into n cells [31]. Starting the procedure with arbitrary values of the electric field E, population densities for electronically excited states, diffusion length Λ_{eff}, and a Treanor-like distribution for the vibrationally excited states [51], the Boltzmann equation is solved by iterations. Then, by using rate coefficients for electron impact processes calculated from the solution to (1), the nonlinear set of equations for electronically excited species and positive ions has been solved by the Newton–Raphson method. The unknown field E and diffusion length Λ_{eff} are varied to satisfy simultaneously equation (3) and the boundary condition for the ion velocity. As a result, a self-consistent solution for

Table 4. Rate constants for reactions involving positive ions.

Reaction		Rate constant (m^3 s^{-1})	References
$N_2(A\,^3\Sigma_u^+) + N_2(a'\,^1\Sigma_u^-)$	$\nearrow N_2^+ + N_2 + e$ $\searrow N_4^+ + e$	$K_{as1} = 1.5 \times 10^{-17}$	[35]
$N_2(a'\,^1\Sigma_u^-) + N_2(a'\,^1\Sigma_u^-)$	$\nearrow N_2^+ + N_2 + e$ $\searrow N_4^+ + e$	$K_{as2} = 1.0 \times 10^{-17}$	[35]
$N_4^+ + N_2 \rightarrow N_2^+ + 2N_2$		$2.1 \times 10^{-22} \exp(T_g/121)$	[35, 46]
$N_2^+ + N \rightarrow N^+ + N_2$		$7.2 \times 10^{-19} \exp(T_g/300)$	[46]
Three-body collisions			
$N_2^+ + N_2 + N_2 \rightarrow N_4^+ + N_2$		5.0×10^{-29} cm^6 s^{-1}	[35]

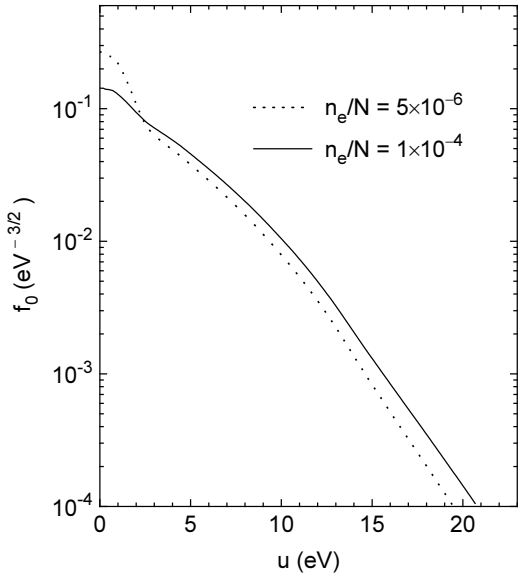

Figure 1. Influence of the degree of ionization on the EEDF (p = 0.6 Torr).

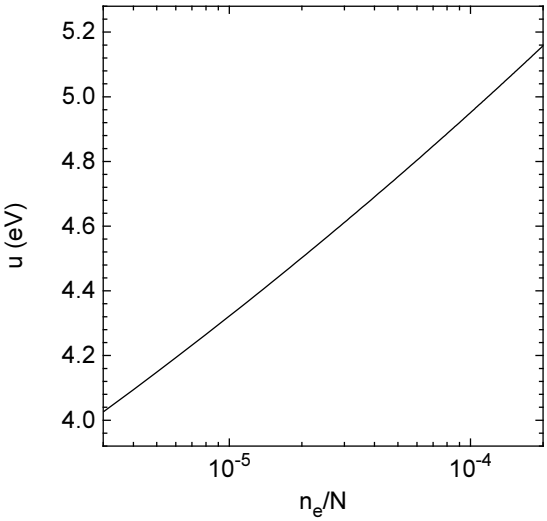

Figure 2. Influence of degree of ionization variations on the average electron energy (p = 0.6 Torr).

Table 5. Rate constants for dissociative recombination of ions.

Reaction	Rate constant (m^3 s^{-1})	Ref.
$e + N_2^+ \rightarrow N + N$	$\alpha_{r1} = 4.8 \times 10^{-13}(300/T_e)^{1/2}$	[37]
$e + N_4^+ \rightarrow N_2 + N_2$	$\alpha_{r2} = 2.0 \times 10^{-12}(300/T_e)^{1/2}$	[37]

the EEDF, the population densities of electronically excited states and positive ions, and the discharge maintaining field is obtained. The set of nonlinear equations for the vibrational population of the electronic ground state is then solved using the electron rates obtained from the EEDF. The above entire cycle is then repeated until a convergent solution is obtained. The final result is a fully self-consistent solution for the EEDF, population densities of all excited species, and discharge maintaining field.

As previously mentioned, n_e/N is taken as an independent parameter since it can be externally controlled by changing the power supplied to the discharge. The neutral gas density N is derived from the ideal gas law assuming a gas temperature $T_g = 1000$ K, a typical value under the present operating conditions.

3. Results and discussion

3.1. Electron kinetics

3.1.1. Influence of the degree of ionization. Figure 1 shows the influence of the degree of ionization on the EEDF for a pressure of 0.6 Torr. For low degree of ionization, the general shape of the distribution is mainly ruled by electron–molecule energy exchanges. A decrease in the EEDF in the energy range of 1.5–3 eV is observed. As is well known, this behaviour reflects the rapid rise of the vibrational cross-sections which increase by approximately two orders of magnitude in this energy range. The effects of this vibrational barrier on the EEDF are however partly attenuated by superelastic collisions which further contribute to enhance the high-energy tail. It should be noted that the effects of superelastic collisions are not determined by the whole vibrational distribution, for all v, but only by the population in the lowest vibrational levels. With increasing n_e/N not only superelastic collisions but also electron–electron collisions 'heat up' the EEDF which results in an increase in the mean electron energy (figure 2)

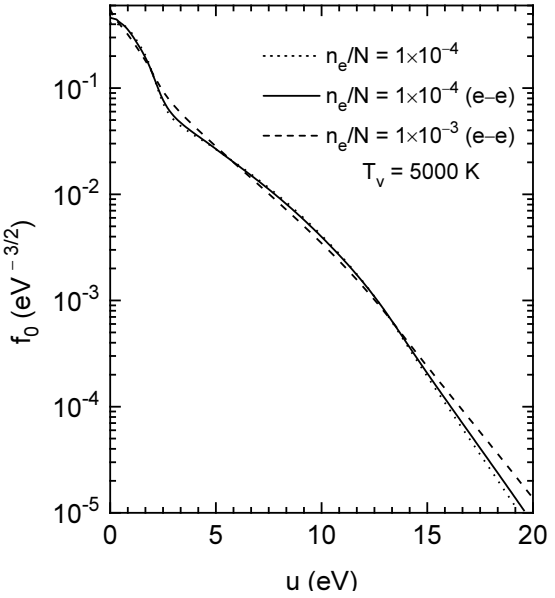

Figure 3. Influence of electron–electron collisions on the EEDF (p = 1 Torr).

and a decrease in the discharge maintaining field (see figure 4, below).

The comparison between various collision frequencies which are important in the establishment of the electron energy spectrum shows that for degree of ionization $n_e/N > 10^{-4}$ the inequality $\nu_{ee} > \nu_v$ holds (ν_{ee} is the electron–electron collision frequency [13], ν_v is the frequency for vibrational excitation or de-excitation). Thus, competitive processes of energy exchange between electrons become important for n_e/N greater than 10^{-4} so the EEDFs calculated without and with electron–electron collisions (for a constant vibrational excitation at T_v = 5000 K) start differing as seen from figure 3. The differences increase with n_e/N as expected. For $n_e/N = 10^{-3}$ the EEDF is almost Maxwellian.

Figure 4 shows the changes in the maintaining field as a function of the ionization degree. Owing to superelastic and electron–electron collisions, lower values of E are needed at higher n_e/N as a consequence of the increase in the ionization rate. The increase in the latter is due, in particular, to the onset of associative ionization as the electronic metastable populations increase. Figure 5 shows that the ionization for low pressures and degree of ionization (high E/N) is controlled by the direct electron impact while for $n_e/N > 3\times10^{-5}$ the associative ionization becomes predominant. As shown in figure 6, the losses are mainly due to diffusion at low n_e/N but become controlled by dissociative recombination for $n_e/N > 8 \times 10^{-5}$.

3.1.2. Influence of the gas pressure. In figure 7, the EEDF is plotted for two different pressures intended for experimental studies. Here, the degree of ionization is kept constant, $n_e/N = 3 \times 10^{-5}$. Note that in order to keep n_e/N = constant at various pressures, different powers supplied to the discharge are necessary. The self-consistently determined values of the maintaining electric

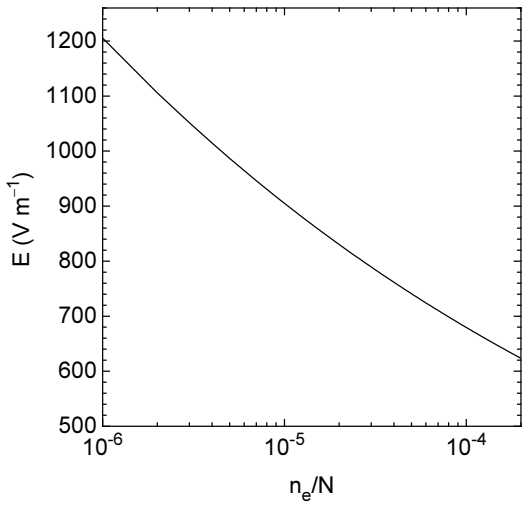

Figure 4. Influence of the degree of ionization on the maintenance electric field strength (p = 0.6 Torr).

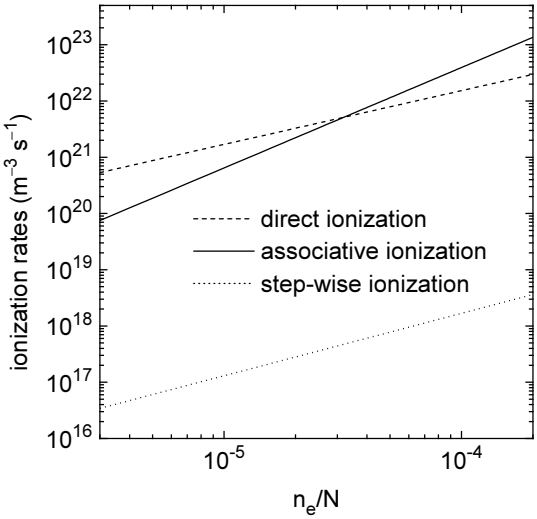

Figure 5. Variations of different channels of ionization as a function of the degree of ionization (p = 0.6 Torr).

field vary from 782 V m^{-1} to 1442 V m^{-1} when the pressure (respectively N) is changed in the range 0.3–2 Torr (figure 8). Consequently, E/N varies from 2.769×10^{-19} V m^2 to 0.465×10^{-20} V m^2. Despite the increase in E with increasing gas pressure, the increase in N results in a lower reduced maintaining field E/N. As E/N decreases, the power input per electron decreases and so does the mean electron energy as shown in figure 9.

The calculated rates of ionization through different channels are shown in figure 10. The results reveal that for the gas discharge operating conditions considered ($n_e/N = 3 \times 10^{-5}$) the ionization rate is primarily determined by associative ionization collisions involving $N_2(A\,^3\Sigma_u^+)$ and $N_2(a'\,^1\Sigma_u^-)$ metastable states, for pressures above 0.7 Torr. The associative ionization increases nonlinearly with pressure (figure 10) due to the absolute increase in the population of $N_2(A\,^3\Sigma_u^+)$ and $N_2(a'\,^1\Sigma_u^-)$. Since n_e/N = constant here, the increase in electron density as

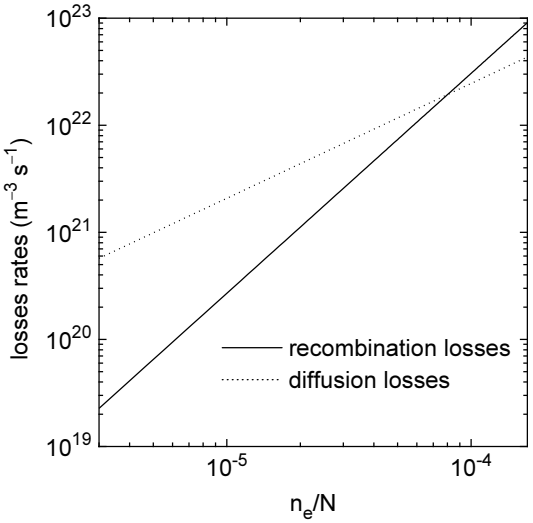

Figure 6. Channels of losses as a function of the degree of ionization (p = 0.6 Torr).

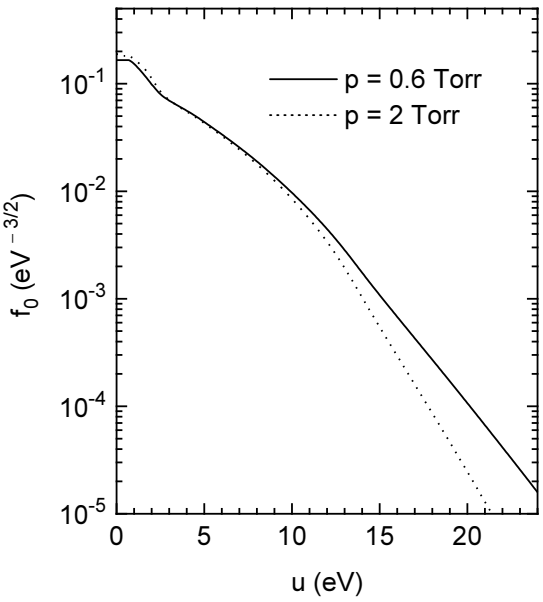

Figure 7. EEDFs at various pressures ($n_e/N = 3 \times 10^{-5}$).

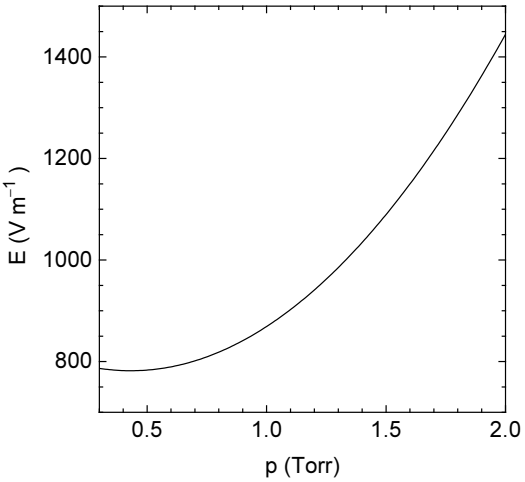

Figure 8. Maintenance electric field strength versus gas pressure variations ($n_e/N = 3 \times 10^{-5}$).

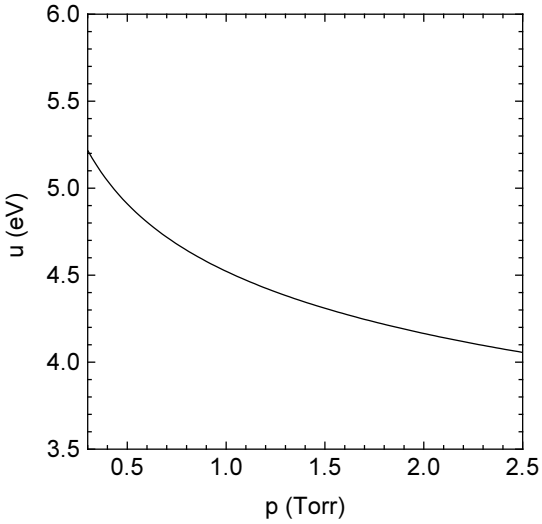

Figure 9. Average electron energy versus gas pressure variations ($n_e/N = 3 \times 10^{-5}$).

the pressure increases has been taken into account.

The step-wise ionization flux (involving $N_2(A\,^3\Sigma_u^+)$, $N_2(a'\,^1\Sigma_u^-)$, and $N_2(B\,^3\Pi_g)$ states) increases with pressure, but its contribution to the total ionization flux is negligible. The processes of direct electron impact ionization are competitive only at lower pressures ($p < 1$ Torr), when E/N is sufficiently high. For pressures $p > 1$ Torr, the recombination losses start to dominate over those by ambipolar diffusion (figure 11).

3.2. Heavy-particle kinetics

3.2.1. Vibrational distribution function. Figures 12 and 13 depict the vibrational distribution functions of nitrogen molecules in the electronic ground state $N_2(X\,^1\Sigma_g^+)$ self-consistently determined with the electron energy distribution functions shown in figures 1 and 7, respectively. The results illustrate the changes in the VDFs (δ_v) for various degrees of ionization (figure 12) and pressures (figure 13). For a higher degree of ionization ($n_e/N = 10^{-4}$) the VDFs are considerably 'excited'. In order to characterize the degree of vibrational excitation (as in [20–22]) we define the vibrational temperature T_v as a characteristic vibrational temperature of a Treanor-like distribution that best fits the calculated fractional populations for $0 \leq v \leq 3$. As pointed out in [20], although the definition of T_v involves only populations in the lowest three levels, once T_v is given the entire VDF becomes in fact uniquely determined. The vibrational temperature of $N_2(X\,^1\Sigma_g^+)$-molecules increases with n_e/N and reaches unusually high values ($\sim$19 000 K) for the highest degrees of ionization considered. This is partly a consequence of the large V–V pumping rates obtained for a gas temperature

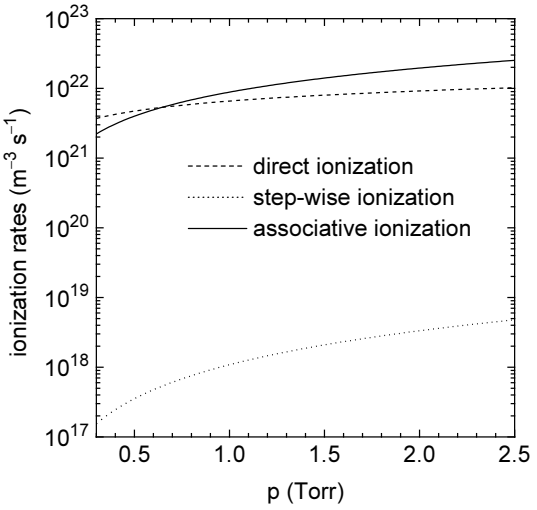

Figure 10. Variations of rates of ionization as a function of the pressure ($n_e/N = 3 \times 10^{-5}$).

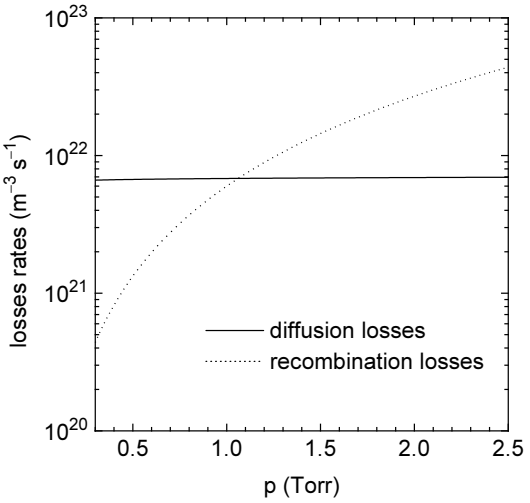

Figure 11. Variations of rates of losses as a function of the pressure ($n_e/N = 3 \times 10^{-5}$).

of 1000 K. Due to this high gas temperature, the shape of the VDF is also considerably different from that typically observed at lower temperatures as, for example, under DC discharge conditions (see below).

A decrease of the vibrational temperature from 16 000 K to 14 500 K is registered as the pressure is increased up to 2 Torr, due to the decrease in the electron rate coefficients for vibrational excitation.

Usually, different regimes of population and depopulation of nitrogen vibrational levels can be clearly identified from the shape of the VDF. This shape results from the combined effects of e–V and V–V exchanges at low v levels, of near-resonant V–V exchanges at intermediate levels, which tend to form a plateau in that region, and to the simultaneous effects of vibrational dissociation and V–T exchanges at the highest levels. However, the VDFs calculated in this work show a distinct change in slope at about $v = 20$, with no apparent plateau being formed, which indicates a transition from the population mechanism

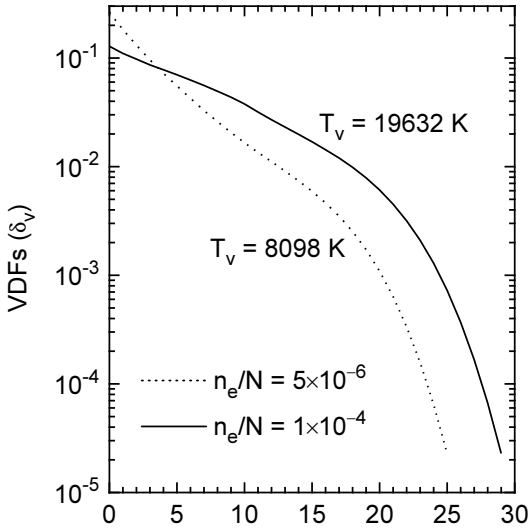

Figure 12. Vibrational distribution function (VDF) of the $N_2(X\,^1\Sigma_g^+)$ state for different degrees of ionization (p = 0.6 Torr).

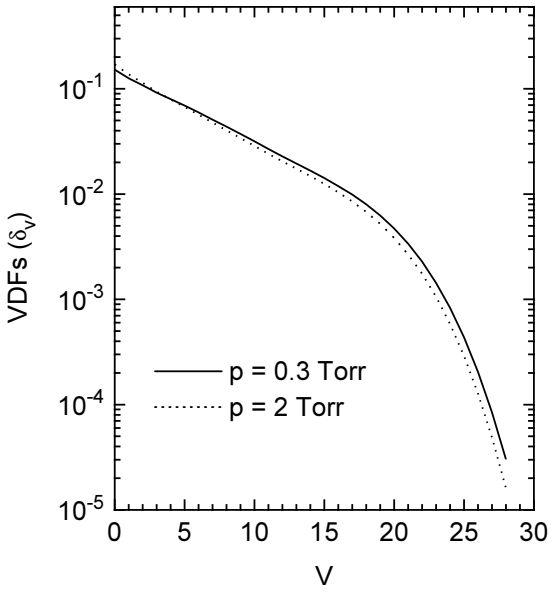

Figure 13. Vibrational distribution function of the $N_2(X\,^1\Sigma_g^+)$ state for different pressures ($n_e/N = 3 \times 10^{-5}$).

by near-resonant V–V exchanges to the V–T depopulating regime. This is a consequence of the high value of $T_g = 1000$ K used here in comparison to previous works, which leads to higher depopulation rates by N_2–N collisions (note that these rates strongly increase with the gas temperature). These effects are extremely important, even for relative atom concentrations as small as 10^{-2}, causing a rapid fall-off in the VDF for $v > 20$. Figure 14 shows that the V–T rates for N_2–N collisions increase with the vth quantum number by several orders of magnitude at the considered temperature. As a result, the typical plateau for intermediate v levels does not occur here and the VDF sharply falls off due to V–T deactivation in collisions with nitrogen atoms [33, 34]. The dissociation by V–V and V–T processes is negligibly small due to this sharp fall-off.

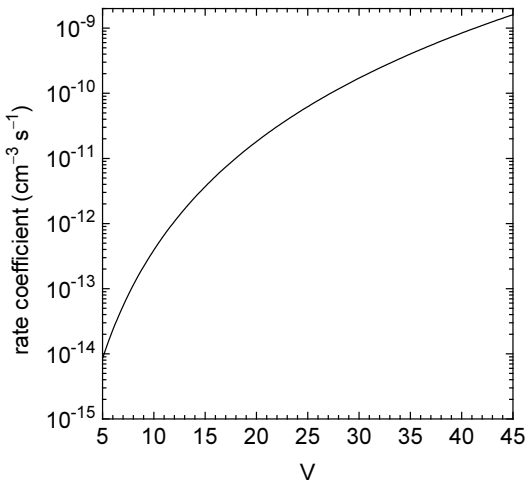

Figure 14. Rate coefficients for V–T exchanges in N_2–N collisions.

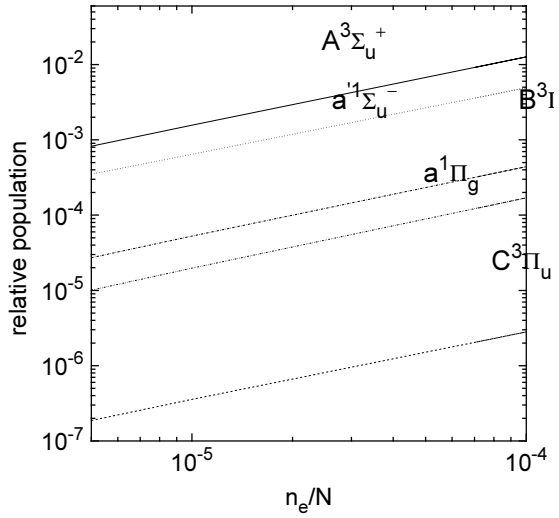

Figure 15. Relative population of electronically excited states as a function of the degree of ionization (p = 0.6 Torr).

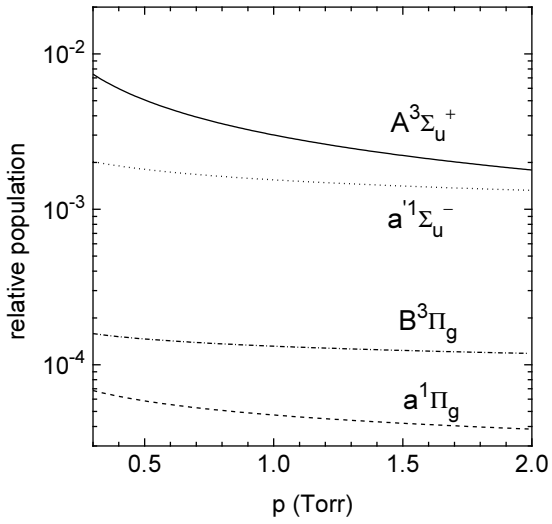

Figure 16. Relative population of electronically excited states as a function of the pressure ($n_e/N = 3 \times 10^{-5}$).

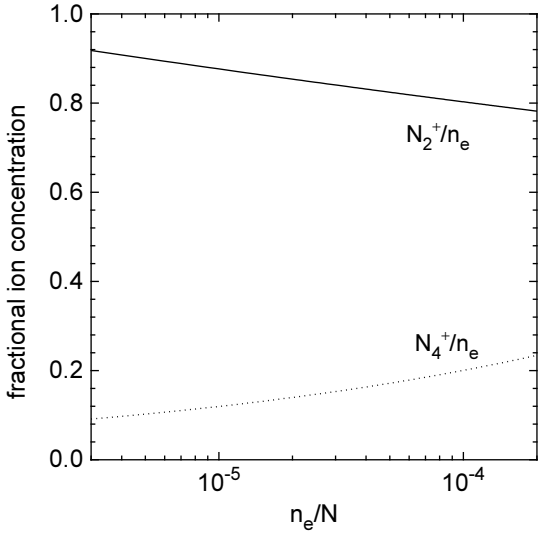

Figure 17. Fractional concentrations of positive ions as a function of the degree of ionization (p = 0.6 Torr).

3.2.2. Electronically excited molecules. The dependence of electronically excited particle densities on the degree of ionization and gas pressure is plotted in figures 15 and 16 respectively. The enhancement of the high-energy part of the EEDF due to superelastic and electron–electron collisions favors electron impact excitation. Since this mechanism is the main source for producing electronically excited species, the excited relative populations increase with n_e/N. The decrease in these populations as the pressure increases is caused by the decrease in the reduced field E/N and, hence, in the excitation rate coefficients. The stronger decrease in the relative population of $N_2(A\,^3\Sigma_u^+)$ observed in figure 16 is due to quenching by nitrogen atoms, whose concentration was assumed to grow with pressure (recall that a constant degree of dissociation has been assumed in the calculations).

3.2.3. Positive ions. Two kinds of positive ion are considered in the present work, N_2^+ and N_4^+. The N_2^+ ions are principally created by electron impact and associative ionization, while associative ionization is the main source of N_4^+ ions. The greater recombination coefficient (see table 5) determines a faster bulk destruction of N_4^+. The variations in the relative ion densities (normalized to the electron density) with the degree of ionization (figure 17) and the pressure (figure 18) depend on the predominant ionization and loss channels under our conditions (see figures 5, 6, 10 and 11 for various ionization and loss channels). When the associative ionization flux increases, the relative concentration of N_4^+ increases too. However, since bulk recombination becomes the dominant loss channel at high n_e/N, the faster recombination of N_4^+ makes that its concentration always keeps small as compared to that of N_2^+. Remember that, due to the lack of data, we have

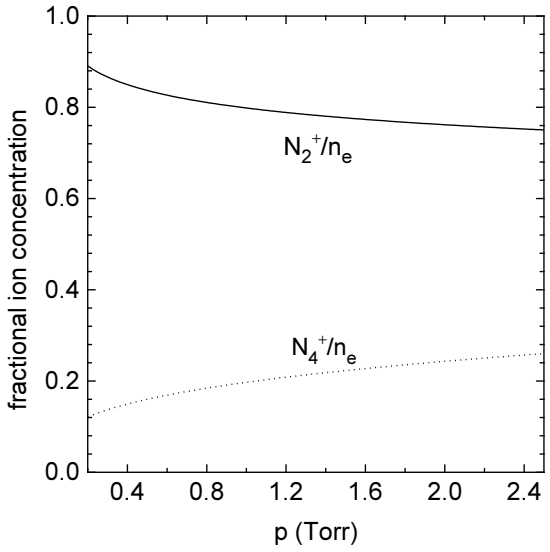

Figure 18. Fractional concentrations of positive ions as a function of the pressure ($n_e/N = 3 \times 10^{-5}$).

assumed the same branching ratio for the production of N_2^+ and N_4^+ by associative ionization, so that figures 17 and 18 should be regarded as merely indicative.

4. Experimental details

4.1. Experimental conditions and procedures

The experiment has been performed in a stationary high-frequency discharge created by a travelling azimuthally symmetric surface wave of frequency $\omega/2\pi = 500$ MHz. The surface wave is excited by a surfatron whose design is described in detail in the review paper by Moisan and Zakrzewski [52]. The plasma column is sustained in nitrogen at pressures of 0.3–1 Torr, in a cylindrical Pyrex tube with relative permittivity $\varepsilon_d = 4.4$ and a 2.25 cm inner radius. The power applied from the generator is $P \in 80$–250 W. A Langmuir probe technique has been used for determining the EEDF and related integral quantities. With regard to the fact that the surface-wave discharge is electrodeless, the probe circuit consists of a small tungsten probe (with length $l_p = 3.2$ mm and radius $R_p = 0.05$ mm) and a large-area electrode (used as an emissive probe [53]). The large electrode is placed inside the surfatron [14]. Following the results in [14], in order to reduce the perturbation caused by the probe as an inhomogeneity in the waveguide, the measuring probe as well as its supply line are directed perpendicular to the discharge axis.

The isotropic part of the EEDF, $f_0(u)$, is related to the second derivative of the current–voltage probe characteristic via the Druyvesteyn formula [54]

$$f_0(u) = \text{constant}\,\frac{\mathrm{d}^2 I_e}{\mathrm{d}U^2} \qquad \text{with } U = U_s - U_p$$

where U_p is the potential applied to the probe, U_s is the plasma potential and I_e is the electron current collected by the probe. The value of the plasma potential, which is necessary to obtain the zero point in the energy scale, is taken at the zero-cross-point position of the second derivative [55]

A passive method of compensation (like in [14]) has been applied to avoid the high-frequency field influence on the probe measurements. The measuring system and the method for numerical differentiation of the current–voltage characteristic are discussed in detail in a former work by Dias [56].

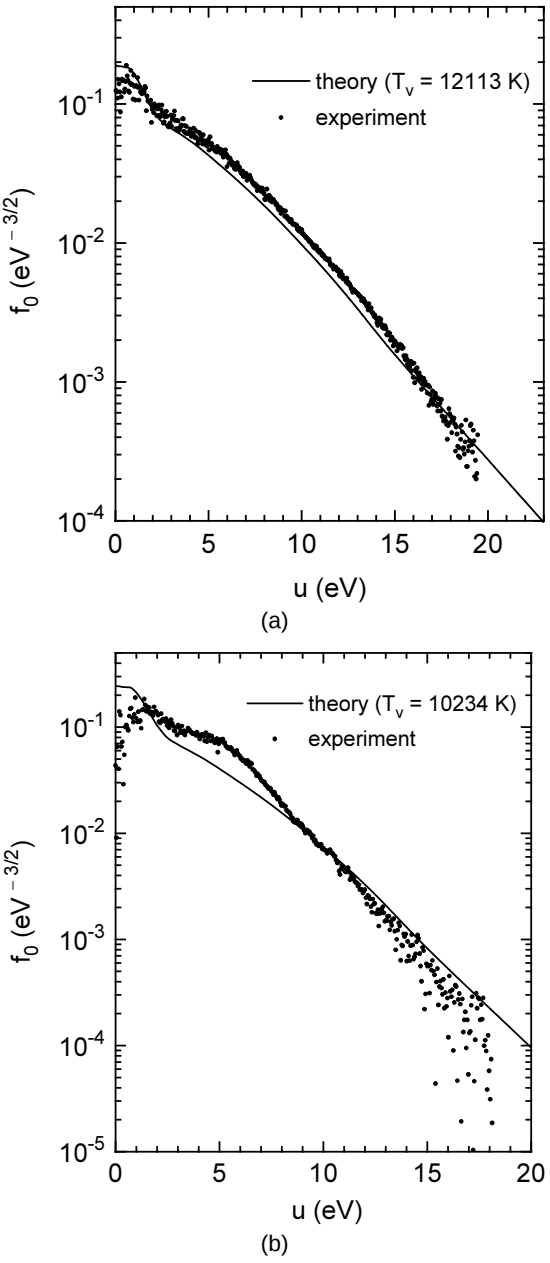

Figure 19. Comparison of experimentally determined EEDFs ($\omega/2\pi$ = 500 MHz, R = 2.25 cm) with the theoretical ones: (a) p = 0.3 Torr, $n_e/N = 1 \times 10^{-5}$; (b) p = 0.5 Torr, $n_e/N = 6 \times 10^{-6}$.

4.2. Comparison between theory and experiment

The experimental results presented in this section are intended to test the general trends of the EEDF and its

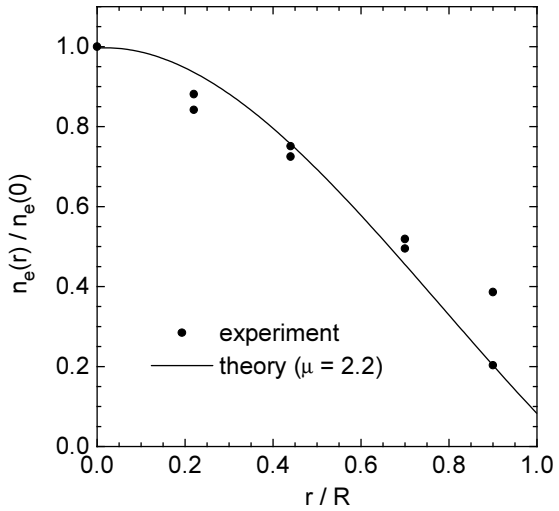

Figure 20. Comparison of experimentally obtained electron density profile ($\omega/2\pi$ = 500 MHz, R = 2.25 cm) with the theoretical one (p = 0.5 Torr).

moments as predicted by the model.

In figure 19, typical experimentally determined EEDFs are compared with model calculations. The scattered measured values at low and high energies indicate the limits of accuracy of the technique, but a dynamic range of nearly three orders of magnitude was reached as seen from the figure.

As predicted, the experimental EEDFs deviate from a Maxwellian distribution. An important experimental result is that the shape of the low-energy part of the measured distribution seems to confirm the important influence of electron collisions of the first and second kind with vibrationally excited nitrogen molecules, as well as the existence of a high degree of vibrational excitation in the electronic ground state. The predicted vibrational temperatures are 12 113 K and 10 234 K for the conditions of figures 19(a) and 19(b) respectively.

Qualitatively, the predicted and measured EEDFs agree well and are similar in shape, apart from deviations observed in the low-energy part of the distributions. It should be stressed that there are no fitting parameters in the theory. For instance, the electric field, which has a great influence on the shape of the EEDF, was determined self-consistently. The degree of ionization n_e/N, an input parameter of the model, is obtained from measurements.

The observed discrepancies at low energies may be attributed to various experimental draw-backs, the well known uncertainty in the choice of plasma potential being the most serious problem. The experimental determination of the EEDF is sensitive to distortions in the vicinity of the zero-cross-point of the second derivative. Many causes, such as the effects of plasma depletion caused by electron sinks on the probe (which occur for finite R_p/λ_e, λ_e denoting the electron mean free path), the high-frequency field influence, the neglect of plasma resistance, the existence of low-frequency fluctuations etc, can affect the accuracy of probe diagnostics in the considered energy range, leading to a suppression of the second derivative peak or to its broadening. The relative error due to the neglect of plasma resistance is approximately $10R_p/\lambda_e$ [14]. For a Maxwellian distribution, this error is estimated to be of the order of 60% in the energy interval of 0–2 eV.

As emphasized in [14] and [55], the voltage gap between the maximum and the zero cross-point of the second derivative is a sensitive indicator for the overall quality of the experiment. For a good quality experiment this gap should not exceed $(0.2–0.3)\langle u\rangle$. In our case, due to the convenient probe arrangement used, a voltage gap less than 1.5 V was obtained. Accordingly, a possible shift in the energy scale of the measured distributions of about 1 eV may be expected.

Another possible source of discrepancy may be the assumption of $T_g = 1000$ K used in calculations. A higher/lower gas temperature at the probe location corresponds to a lower/higher neutral density, which would yield differences between the measured and calculated tail of the EEDF.

Figure 20 shows the radial profile of the electron density for $p = 0.5$ Torr, $n_e/N = 6 \times 10^{-6}$. These results were obtained at various radial positions from the ion saturation probe current for large applied negative voltage. Also plotted for comparison is the profile

$$n_e(r) = n_e(0)J_0(r/\Lambda_{\text{eff}}) = n_e(0)J_0(\mu r/R)$$

for a value of $\mu = 2.2$ derived from the model under our discharge conditions. It is seen that the latter profile agrees quite well with the measurements.

5. Conclusion

In this paper, we have presented a self-consistent kinetic model of a surface-wave-sustained nitrogen plasma. The model is based on a set of coupled equations consisting of the electron Boltzmann equation in the well known Lorentz approximation and the rate balance equations for the most important excited species—vibrationally $N_2(X\,^1\Sigma_g^+, v)$ and electronically $N_2(A\,^3\Sigma_u^+, a'\,^1\Sigma_u^-, B\,^3\Pi_g, a\,^1\Pi_g, C\,^3\Pi_u)$ excited states—and charged particles (N_2^+, N_4^+) in the discharge. Electron collisions with nitrogen molecules of the first and second kind and electron–electron collisions are accounted for in the Boltzmann equation. The field strength necessary for a steady-state operation of the discharge is obtained from the balance between the total rate of ionization, including associative, direct and step-wise processes, and the total rate of electron losses due to diffusion to the wall and bulk recombination. The basic set of equations is solved in a self-consistent manner by an iterative procedure.

The model determines, as a function of the discharge operating parameters, the EEDF, the radially averaged populations in the vibrational levels of the electronic ground state $N_2(X\,^1\Sigma_g^+)$, the population densities of the most important electronic states $N_2(A\,^3\Sigma_u^+, a'\,^1\Sigma_u^-, B\,^3\Pi_g, a\,^1\Pi_g, C\,^3\Pi_u)$, and the concentration of N_2^+ and N_4^+ ions, self-consistently with the discharge maintaining electric field. Furthermore, a quantitative comparison between experimental data and theoretical predictions has been performed.

On the basis of the results obtained one can draw the following conclusions:

(i) Under usual operating conditions for a surface-wave-sustained discharge at low pressures, the general shape of the EEDF is mainly ruled by electron–molecule energy exchange processes. The influence of electron–electron collisions for the achieved degrees of ionization is negligible; energy exchanges between electrons become competitive only when n_e/N is greater than 10^{-4}.

(ii) With increasing n_e/N, superelastic collisions of electrons with vibrationally excited molecules and electron–electron collisions 'heat up' the EEDF and lead to an increase in the average electron energy and a decrease in the discharge sustaining electric field.

(iii) The EEDF behaviour is strongly correlated to the high degree of vibrational excitation of the electronic ground state. The vibrational temperature of $N_2(X\,^1\Sigma_g^+)$ molecules increases with the degree of ionization, reaching high values (19 000 K) for high degrees of ionization ($p = 0.6$ Torr, $n_e/N = 1 \times 10^{-4}$), for the gas temperature of 1000 K considered here.

(iv) The effects of V–T processes in N_2–N collisions cause a rapid fall-off in the vibrational distribution function even at relatively low vibrational quantum numbers. Accordingly, the plateau region in the VDF virtually disappears.

(v) For the range of operating parameters $p \in 0.6$–2 Torr, $n_e/N > 3 \times 10^{-5}$, the ionization rate is primarily determined by associative ionization in collisions involving $N_2(A\,^3\Sigma_u^+)$ and $N_2(a'\,^1\Sigma_u^-)$ metastable states.

(vi) The comparison between experimental results and the self-consistently determined EEDF and its moments reveals a satisfactory agreement.

(vii) The theoretical prediction of a high degree of vibrational excitation in the electronic ground state is indirectly confirmed by the shape of the experimental EEDF.

This work has, nevertheless, some weaknesses. A main assumption of the model is the validity of the 'thin-cylinder approximation', i.e. a radial homogeneity of the high-frequency field was considered. In future work, the formalism developed here should be extended to include the discharge electrodynamics. In fact, a detailed and accurate modelling requires a self-consistent determination of both the plasma parameters and the electrodynamic characteristics of the travelling surface wave. Furthermore, a comparison of theoretical and experimental results demands a better knowledge of the gas temperature. The model should include also the kinetics of nitrogen atoms, whose concentration was only estimated here and treated as an external parameter.

In conclusion, the present theoretical model is satisfactory inasmuch as it provides physical insight into the basic workings on surface-wave discharges in nitrogen. A model including also the surface wave discharge electrodynamics is now in progress and will be reported elsewhere.

Acknowledgments

We have benefited from useful discussions with Professor B F Gordiets. This work was performed under a PRAXIS XXI Research Grant by the Portuguese Ministry of Science and Technology, with partial support of the FEDER Programme of the European Commission. It was also partially supported by the Bulgarian National Fund for Scientific Research under grant F–471/94. One of the authors (ET) gratefully acknowledges NATO for the award of a research fellowship.

References

[1] Moisan M and Zakrzewski Z 1986 *Radiative Processes in Discharges* ed J M Proud and L H Luessen (New York: Plenum) p 381
[2] Kortshagen U and Schlüter H 1992 *J. Phys. D: Appl. Phys.* **25** 644
[3] Zethoff M and Kortshagen U 1992 *J. Phys. D: Appl. Phys.* **25** 1574
[4] Ferreira C M 1981 *J. Phys. D: Appl. Phys.* **14** 1811
[5] Ferreira C M 1983 *J. Phys. D: Appl. Phys.* **16** 1673
[6] Ferreira C M 1986 *Radiative Processes in Discharges* ed J M Proud and L H Luessen (New York: Plenum) p 431
[7] Boisse-Laporte C, Granier A, Bloyet E, Leprince P and Marec J 1987 *J. Appl. Phys.* **61** 1740
[8] Boisse-Laporte C, Granier A, Dervisevic E, Leprince P and Marec J 1987 *J. Phys. D: Appl. Phys.* **20** 197
[9] Ferreira C M and Moisan M 1988 *Phys. Scr.* **38** 382
[10] Kortshagen U and Schlüter H 1991 *J. Phys. D: Appl. Phys.* **24** 1585
[11] Sá A B, Ferreira C M, Pasquiers S, Boisse-Laporte C, Leprince P and Marec J 1991 *J. Appl. Phys.* **70** 4147
[12] Kortshagen U 1993 *J. Phys. D: Appl. Phys.* **26** 1230
[13] Kortshagen U, Shivarova A, Tatarova E and Zamfirov D 1994 *J. Phys. D: Appl. Phys.* **27** 311
[14] Grosse S, Schlüter H and Tatarova E 1994 *Phys. Scr.* **50** 532
[15] Grosse S, Schlüter H and Tatarova E 1994 *Plasma Sources Sci. Technol.* **3** 545
[16] Zhelyazkov I and Atanassov V 1995 *Phys. Rep.* **255** 79
[17] Tatarova E and Zamfirov D 1995 *J. Phys. D: Appl. Phys.* **28** 1354
[18] Biberman L M, Vorob'ev V S and Iakubov I T 1982 *Kinetics of a Nonequilibrium Low-Temperature Plasma* (Moscow: Nauka) (in Russian)
[19] Nighan W L 1970 *Phys. Rev.* A **2** 1989
[20] Loureiro J and Ferreira C M 1986 *J. Phys. D: Appl. Phys.* **19** 17
[21] Loureiro J and Ferreira C M 1989 *J. Phys. D: Appl. Phys.* **22** 67
[22] Ferreira C M and Loureiro J 1989 *J. Phys. D: Appl. Phys.* **22** 76
[23] Cacciatore M, Capitelli M and Gorse C 1980 *J. Phys. D: Appl. Phys.* **13** 575
[24] Cacciatore M and Capitelli M 1981 *Chem. Phys.* **55** 67
[25] Cacciatore M, Capitelli M and Gorse C 1982 *Chem. Phys.* **66** 141
[26] Capitelli M, Celiberto R, Gorse C, Winkler R and Wilhelm J 1988 *J. Phys. D: Appl. Phys.* **21** 691
[27] Shivarova A and Zhelyazkov I 1982 *Electromagnetic Surface Modes* ed A D Boardman (Chichester: Wiley) Ch 12
[28] Kortshagen U, Schlüter H and Shivarova A 1991 *J. Phys. D: Appl. Phys.* **24** 157
[29] Shkarovsky I P, Johnston T W and Bachinski M P 1966 *The Particle Kinetics of Plasmas* (London: Addison-Wesley)

[30] Sá P A, Loureiro J and Ferreira C M 1992 *J. Phys. D: Appl. Phys.* **25** 960
[31] Dezhen W, Tencai M and Baohai G 1993 *J. Phys. D: Appl. Phys.* **26** 62
[32] Phelps A V and Pitchford L C 1985 *JILA Information Center Report* (Boulder, CO: Colorado University) no 26
[33] Guerra V and Loureiro J 1995 *J. Phys. D: Appl. Phys.* **28** 1903
[34] Guerra V and Loureiro J 1997 *Plasma Sources Sci. Technol.* **6** 361
[35] Gordiets B F, Ferreira C M, Guerra V L, Loureiro J M A H, Nahorny J, Pagnon D, Touzeau M and Vialle M 1995 *IEEE Trans. Plasma Sci.* **PS-23** 750
[36] Piper L G 1987 *J. Chem. Phys.* **87** 1625
[37] Kossyi I A, Kostinsky A Yu, Matveyev A A and Silakob V D 1992 *Plasma Sources Sci. Technol.* **1** 207
[38] Keck J and Carrier G 1965 *J. Chem. Phys.* **43** 2284
[39] Calo J M and Axtmann R C 1971 *J. Chem. Phys.* **54** 1332
[40] Marrinelly W J, Kessler W J, Green B D and Blumberg W A M 1989 *J. Chem. Phys.* **90** 2167
[41] Freund N S 1972 *J. Chem. Phys.* **56** 4344
[42] Kimura T, Akatsuka K and Ohe K 1994 *J. Phys. D: Appl. Phys.* **27** 1664
[43] Piper L G 1988 *J. Chem. Phys.* **88** 6911
[44] Clark W G and Setser D W 1980 *J. Chem. Phys.* **84** 2225
[45] Gilmore F R, Bauer E and McGowan J W 1969 *J. Quant. Spectrosc. Radiat. Transfer* **9** 157
[46] Slovetskii D I 1980 *Mechanisms of Chemical Reactions in a Non-Equilibrium Plasma* (Moscow: Nauka) (in Russian)
[47] Golant V E, Zhilinsky A P and Sakharov I E 1980 *Fundamentals of Plasma Physics* (New York: Wiley)
[48] McDaniel E W and Mason E A 1973 *The Mobility and Diffusion of Ions in Gases* (New York: Wiley)
[49] Garscadden A and Nagpal R 1995 *Plasma Sources Sci. Technol.* **4** 268
[50] Benilov M S 1996 *J. Phys. D: Appl. Phys.* **29** 364
[51] Treanor C E, Rich J W and Rehm R G 1968 *J. Chem. Phys.* **48** 1798
[52] Moisan M and Zakrzewski Z 1991 *J. Phys. D: Appl. Phys.* **24** 1025
[53] Dias F M 1993 *Microwave Discharges: Fundamentals and Applications* ed C M Ferreira and M Moisan (New York: Plenum) p 291
[54] Druyvesteyn M J 1930 *Z. Phys.* **64** 781
[55] Godyak V A, Piejak R B and Alexandrovich B M 1992 *Plasma Sources Sci. Technol.* **1** 36
[56] Dias F M 1995 *Plasma Sources Sci. Technol.* **4** 86